Nanoscale

ROYAL SOCIETY OF CHEMISTRY

PAPER

View Article Online
View Journal | View Issue

Check for updates

Cite this: *Nanoscale*, 2021, **13**, 9264

Emerging flat bands in large-angle twisted bi-layer graphene under pressure†

Liangbing Ge,[a] Kun Ni,*[a,b] Xiaojun Wu, [a] Zhengping Fu, [a,c] Yalin Lu[a,c] and Yanwu Zhu *[a,b]

Received 13th January 2021,
Accepted 18th April 2021

DOI: 10.1039/d1nr00220a

rsc.li/nanoscale

Recent experiments on magic-angle twisted bi-layer graphene have attracted intensive attention due to exotic properties such as unconventional superconductivity and correlated insulation. These phenomena were often found at a magic angle less than 1.1°. However, the preparation of precisely controlled bi-layer graphene with a small magic angle is challenging. In this work, electronic properties of large-angle twisted bi-layer graphene (TBG) under pressure are investigated with density functional theory. We demonstrate that large-angle TBG can display flat bands nearby the Fermi level under pressure, which may also induce interesting properties such as superconductivity which have only been found in small-angle TBG at ambient pressure. The Fermi velocity is found to decrease monotonously with pressure for large twisted angles, *e.g.*, 21.8°. Our work indicates that applying pressure provides opportunities for flat-band engineering in larger angle TBG and supports further exploration in related investigations.

Introduction

Since the exfoliation of high quality graphene in 2004,[1] it has attracted great attention due to its unique electronic,[2] thermal,[3] and mechanical properties.[4] Among its many superior properties, electronic properties are significantly important for the next-generation electronic devices and are strongly dependent on the number and the stacking order of graphitic layers for multilayer graphene.[5–11] By stacking two layers of graphene and rotating them to a certain angle, a novel superlattice called a Moiré pattern will be formed.[12–14] The interaction between the two layers of graphene in the superlattice leads to a series of novel phenomena, particularly for small twisting angles, such as unconventional superconductivity[15] and correlated insulation,[16] pseudo-magnetic fields,[17] orbital magnets,[18] charge order,[19] Chern insulation,[20] *etc*. Furthermore, these phenomena are often related to some unique electronic structures of twisted bi-layer graphene (TBG), such as the appearance of two Van Hove singularities (VHSs) at magic angles,[21–24] the renormalization of Fermi velocity at the Dirac point, and Landau quantization.[25–27] Recently, Cao *et al.* found the Mott insulator behavior and superconducting phase in TBG at a critical temperature of 1.7 K for a twisting angle of around 1.1°.[15,16] This angle has been referred to as a magic angle, corresponding to a Moiré period of ~13.5 nm. The findings provide an additional mechanism for the traditional superconducting materials which has puzzled researchers for decades.[28] Although the interesting findings have attracted intensive interest,[29–32] understanding of the mechanism of superconductivity needs further efforts. At ambient pressure, flat bands are created in TBG when the rotation angle reaches the magic angle, implying an unconventional superconductor phase, which was explained by Padhi *et al.* using a Wigner crystallization model.[33] However in a recent study, the superconductivity observed in TBG has been regarded as a consequence of the Kohn–Luttinger (KL) instability[34] which leads to an effective attraction between electrons with originally repulsive interaction. Apart from these, the researchers also considered the impact of chemical or physical modulations on the properties of TBG, including chemical doping,[35] electric field,[35] pressure,[32,35,36] *etc*. For instance, Yndurain[36] *et al.* theoretically unveiled the possibility of creating magnetic structures in compressed TBG with a larger twist angle, 5.08°. Flat-band angles were found again by Yankowitz and co-workers,[31,37] opening an avenue to creating partially filled bands for angles slightly deviating from magic angles. Very recently, Gao *et al.* demonstrated that a graphene/h-BN Moiré superlattice can open up a band gap of ~70 to 90 meV at the primary Dirac point at a pressure of 8.3 GPa with a twist angle of ~1.8°.[38] Although

[a]*Hefei National Research Center for Physical Sciences at the Microscale, & CAS Key Laboratory of Materials for Energy Conversion, & Department of Materials Science and Engineering, University of Science and Technology of China, Hefei, Anhui 230026, P. R. China. E-mail: nikun@ustc.edu.cn, zhuyanwu@ustc.edu.cn*
[b]*i-ChEM (Collaborative Innovation Center of Chemistry for Energy Materials), University of Science and Technology of China, Hefei, Anhui 230026, P. R. China*
[c]*Anhui Laboratory of Advanced Photon Science and Technology, University of Science and Technology of China, Hefei 230026, P. R. China*

†Electronic supplementary information (ESI) available. See DOI: 10.1039/d1nr00220a

Culchac *et al.* reported flat bands and gaps in ~2°-TBG using the tight-banding method,[39] most of the existing related works focused onto twisting angles of less than 2°; the exciting physical phenomena in TBGs with small twisted angles are not found in larger angles at ambient pressure.[40,41] In fact, pressure plays an important role in modulation of electronic properties with respect to two-dimensional materials.[42,43] A natural question is whether TBGs with larger angles could also show interesting electronic properties under pressure. To the best of our knowledge, attempts on investigating the electronic structure of TBG under high pressures at large angles (more than 9°) are rare.

In this work, we report the emergence of flat bands close to the Fermi level of TBG for higher angles under high pressures with an *ab initio* approach. We show that for twisting angles ranging from above 9° up to nearly 30°, the dispersion relationship of TBG is linearly identical to that of single-layer graphene (SLG) at the K point. However, it drastically changes under external pressure, and their eigenvalue spectra display a flat band around the Fermi level. Consequently, electron correlations take place.

Calculation methods

All our calculations were performed with density functional theory (DFT) as implemented in the Vienna Ab initio Simulation Package (VASP)[44] by using Perdew, Burke, and Ernzerhof (PBE) generalized gradient approximation (GGA)[45] for the exchange–correlation functional.[46] The projector augmented wave[47] potentials were adopted to describe the interaction between ions and valence electrons and to ensure the accuracy of the calculation; the energy cut-off of the plane wave was set to be 500 eV. The relaxation of atomic positions was performed using the conjugated-gradient method until the Hellmann–Feynman force of each atom was smaller than 0.02 eV $Å^{-1}$ and the energy tolerance was 10^{-5} eV. K points sampling of the Brillouin zone was achieved by a Γ-centered method for geometric optimization and static self-consistent-field calculation with reciprocal spacing distances of 0.04 $Å^{-1}$ and 0.025 $Å^{-1}$, respectively. For band structure calculations, the high symmetry point path Γ (0.000, 0.000, 0.000)–M (0.000, 0.500, 0.000)–K (0.333, 0.667, 0.000)–Γ (0.000, 0.000, 0.000) was adopted since the angle between OA and OB of the simulation cell is 60°. As the periodic boundary condition was applied in all three dimensions, the height of the unit cell was set to 16 Å to include enough vacuum to minimize the interaction between adjacent layers. To describe long-range van der Waals interaction between two graphene layers, Grimme's DFT-D3 method[48] was used in all calculations. A Gaussian type smearing of 0.05 eV was used for geometry optimization. For the calculation of density of states, the energy window of smearing was chosen as 0.1 eV. The spin-restricted method was adopted after extensive testing. All the parameter values given above were carefully tested and optimized. Pressure (P) was calculated by $P = F/S$, where F is the sum of the forces on one graphene layer along the Z direction due to the coulombic repulsion, and S is the area of the simulation cell, as widely used in previous studies.[32,36] The interlayer distance of two graphene layers, *e.g.*, on 9.4°-TBG, was reduced from 3.64 Å under ambient conditions to 3.64, 3.24, 2.84 and 2.44 Å to load pressures, corresponding to pressures of 0.0, 5.28, 24.28 and 75.52 GPa, respectively. Note that the Fermi velocity can be deduced from the slope of the dispersions at the Dirac point along the Γ–K direction using the formula $v_F = \frac{1}{\hbar}\frac{\partial E}{\partial k}$, and sampling 120 points within the distance of 0.037 $Å^{-1}$ near by the high symmetry point K for the calculation of Fermi velocity.

Results and discussion

The description of an infinitely large 2D material needs a periodic model, which can only be achieved at a commensurate twisting angle between two graphene layers.[14,40] For this study, we constructed models (see Fig. S1†) for TBGs of four different angles, *i.e.*, 9.4°, 13.2°, 21.8°, and 27.8°, containing 148, 76, 28, and 52 carbon atoms in a unit cell,[49] respectively, from AA-stacked bi-layer graphene (BLG). The axis of rotation passes through the carbon atoms facing up and down. The consideration of small angles leads to a much larger unit cell at a commensurate angle;[49] thus we only consider these four angles because of the limitation of computing resources.

Fig. 1 shows the band structures and density of states of 9.4°-TBG without compression (a separation of 3.64 Å between two layers) or under pressure of 75.52 GPa, respectively. In Fig. 1(a), the linear dispersion appearing in SLG in the vicinity of high-symmetry point K is observed while degenerated by two folds, resulting in fourfold degenerate states from the p_z orbital of the carbon atom, similar to that reported in ref. 32. The shape of the density of states is therefore similar to that of SLG, as shown in Fig. 1(b), which can be attributed to the weak effective interlayer coupling for a larger twist angle.[26,50,51] Two weak peaks, commonly called VHSs flanking,[24] approximately 0.6 eV in energy far away from the Dirac point, are observed as indicated by the black arrows, agreeing well with previous experimental data.[24] After applying a pressure of 75.52 GPa onto BLG, three remarkable features different from the original situation are unveiled as shown in Fig. 1(c and d). Firstly, we can see that the linear dispersion around the K point disappears, which means the massless fermion feature vanishes.[26] Secondly, two bands near the Fermi level split and get flat similar to that found in magic-angle TBG,[15] ascribed to the larger interaction between layers,[13,14,52] due to enhanced coupling and localization of electrons induced by external pressure.[32] In addition, the two peaks close to the Fermi level as indicated by the black arrows are broadened in Fig. 1(d) owing to the emergence of flat bands near the Fermi level.

In order to obtain better knowledge of the electron localization of TBGs under pressure, the electron localization function (ELF) and partial charge density (PCD) of the top valence band and bottom conduction band for 9.4°-TBG at pressures

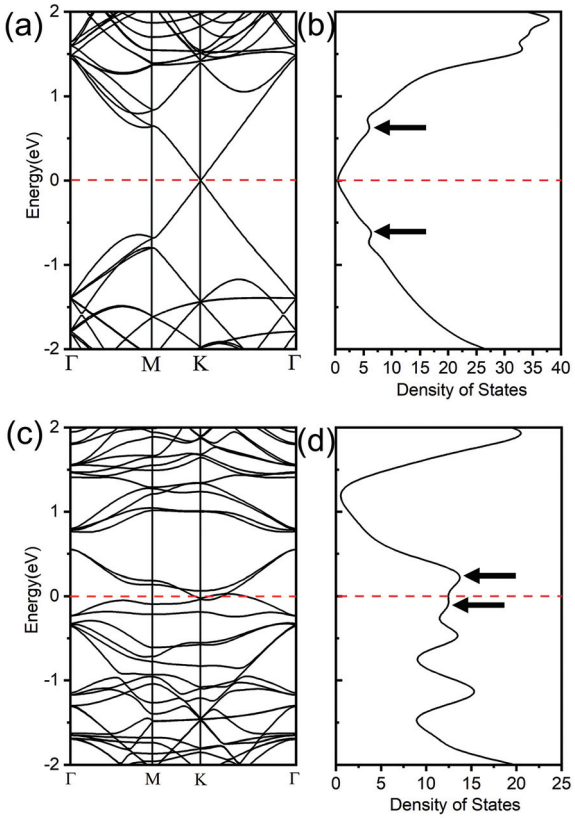

Fig. 1 Band structures and density of states of a unit cell corresponding to a 9.4° angle between the two layers (a and b) without external pressure and (c and d) with a pressure of 75.52 GPa. The black arrows indicate the locations of VHSs.

of 0 GPa and 75.52 GPa have been calculated, as shown in Fig. 2 and Fig. S3.† A two-dimensional slice of the ELF parallel to the graphene layer and located right at the middle of the two layers is considered. The ELF in Fig. 2(a) indicates the electrons are highly delocalized in the interlayer space at ambient pressure, and significantly localized in the interlayer space after applying a pressure of 75.52 GPa due to the enhanced interlayer interaction, as shown in Fig. 2(b). Besides, the PCDs of the top valence band and bottom conduction band of 9.4°-TBG show that the electrons are spread across the graphene layer at 0 GPa in Fig. 2(c) and Fig. S3(a),† respectively, thus indicating a delocalized nature of the electrons, which has been widely reported.[53,54] When a pressure of 75.52 GPa is loaded, the PCDs of the top valence band and bottom conduction band show an obvious gathering of electrons at the AA-stacking region and decreased electron density at the AB-stacking region in Fig. 2(d) and Fig. S3(b),† respectively, indicating a localized nature of the electrons. In addition, the differential charge Δq (see definition in the ESI†) is calculated to describe the charge gathering in real space in each carbon layer. Δq equals 0.17 e^- when P = 75.52 GPa, which reveals a larger unevenness of the charge distribution within the layer, comparing to Δq equaling 0.09 e^- at 0 GPa.

To further verify whether VHSs appear under pressure near the K point, three-dimensional band structures of the valence band maximum (VBM) and conduction band minimum (CBM) in a two-dimensional Brillouin zone (2DBZ) around the K point are shown in Fig. 3(a). Regions 1 and 2 marked with the red dotted frames in Fig. 3(a) indicate the saddle shape regions. To clarify the essential feature of the saddle shape more clearly, the projection mapping of CBM and VBM is shown in Fig. 3(b and c). The saddle point is the maximum in one direction and the minimum in the other direction in the 3D band structure,[55] causing the formation of VHS.[23] Differing from the reported sharp peak at the Fermi level for 5.08°-TBG under 2.19 GPa in ref. 36, our simulation shows a broad peak for 9.4°-TBG under 75.52 GPa. In the past few decades, researchers have considered that the mechanism of high-temperature superconductivity is related to the expansion of VHSs near the Fermi surface.[56–58] In fact, VHSs have been found in high-temperature cuprate superconductors by angular resolu-

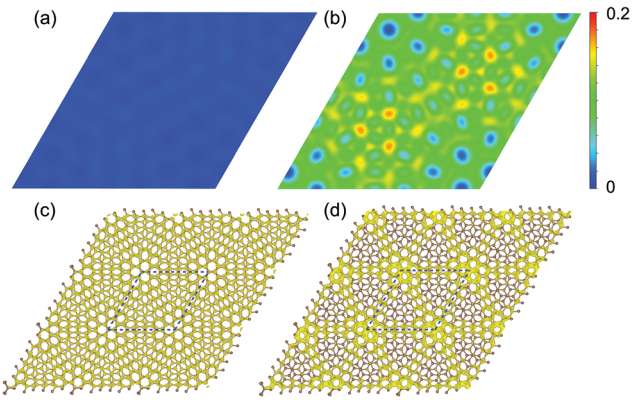

Fig. 2 2D slices of ELF at the middle of the two graphene layers of 9.4°-TBG at pressures of (a) 0 GPa and (b) 75.52 GPa, respectively. PCD of the top valence band for 9.4°-TBG at pressures of (c) 0 GPa and (d) 75.52 GPa, respectively. The dashed line indicates the unit cell of 9.4°-TBG. The iso-surface value is 6 × 10^{-4} e $Bohr^{-3}$.

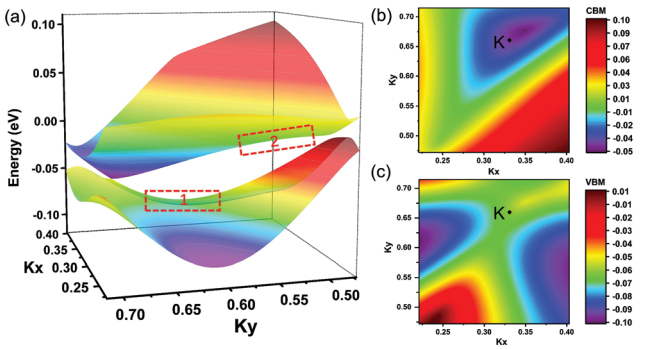

Fig. 3 (a) Three-dimensional band structures of VBM and CBM sampling around the K point for a 9.4° twisted angle under a pressure of ~75.52 GPa. Red regions 1 and 2 show the VHSs at the highest valence band and lowest conduction band, respectively. Projection mapping of the (b) CBM and (c) VBM, in which the black points indicate the location of the K point.

tion photoelectron spectroscopy.[59,60] Superconductivity or some other strong correlated phenomena may be found for these twisting angles under high pressures when experimental conditions are satisfied. Similar features were also discovered for the other three angles under higher pressures, as shown in ESI Fig. S4–7.†

The emergence of a flat band in the electronic structure may be an important character behind many novel and exciting phenomena.[15,16,30,36,56] As described above, the density of electronic states of TBG drastically increases near the Fermi level due to the presence of a flat band under high pressures. We chose the integrated density of states (IDOS) normalized to the number of atoms in a unit cell as a quantitative indicator. Specifically, we have calculated the IDOS in an energy range from −0.2 to 0 eV for four angles under the same pressure of ~46.5 GPa. As shown in Fig. 4(a), the IDOS decreases with the increase in twisting angle, suggesting that the achievement of the flat band for small twisting angles requires relatively smaller pressures. This conclusion matches well with the results in ref. 32, in which pressures of 3.5 GPa for a 1.47° twisting angle and 9.2 GPa for a 2.00° twisting angle were compared. Besides, Y. Cao[15] *et al.* reported superconductivity phenomena in 1.05°-TBG at ambient pressure, and Yankowitz[31] *et al.* further presented the superconductivity and insulating states by applying 2.21 GPa hydrostatic pressure in TBG with larger angle of 1.27°. In addition, Fig. S8† shows the increased IDOS with increasing pressure for different twisting angles, and we could also find that smaller angle benefits the increased IDOS and thus the flat band. It should be pointed out that a flat band scenario has become a fingerprint for the occurrence of superconductivity,[57] thus providing probability in the realization of superconductivity in larger angle TBGs under pressure.

The Fermi velocity is a good measurement of the degree of electron localization. As we know, the wave function of electrons in graphene possesses unique behaviors such as chirality and the Klein paradox, implying that the electrons in graphene are mostly delocalized. The localization and dependence of the Fermi velocity of localized electrons on angles in TBG were reported theoretically in ref. 26. Pressure may act as another knob for realizing the scenario. In Fig. 4(b), the ratio of the Fermi velocity at the Dirac point in compressed TBG to the Fermi velocity in SLG is plotted as a function of external pressure. We can see that v_F is almost the same as that in SLG without external pressure, confirming the relatively weak coupling in the bilayer graphene at ambient pressure. For the whole range of the pressures considered, the Fermi velocity shows a monotonic decrease, indicating the increasing localization of electrons with pressure.[26] As a result, the electron kinetic energy might exceed the scale of the two-particle Coulomb interaction, leading to correlated behavior.

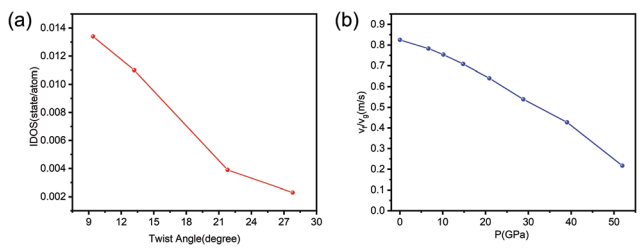

Fig. 4 (a) Integrated density of states (IDOS) normalized to the number of atoms in a unit cell for four twisting angles under a pressure of ~46.5 GPa. (b) Change in the Fermi velocity (v_F) at the Dirac point with pressure in 21.8°-TBG, normalized to v_g; the Fermi velocity for perfect graphene is ~10^6 m s^{-1}.

Conclusions

In summary, we performed *ab initio* calculations to explore the electronic properties of TBGs under pressure for four large twisting angles. We showed that applying external pressure induces the appearance of flat bands and VHSs near the Fermi level in large angle TBGs. Our study indicated that the emergence of flat bands at low angles requires relatively smaller pressures. We also demonstrated that the Fermi velocity is reduced with pressure, suggesting the increasing localization of electrons and enhanced correlation. Applying hydrostatic pressure may provide opportunities for flat-band engineering in large angle TBGs, supporting further experimental exploration.

Conflicts of interest

There are no conflicts to declare.

Acknowledgements

This work was supported by the National Key R&D Program of China (grant no. 2020YFA0711502, 2016YFA0401004), the Natural Science Foundation of China (51772282, 51972299, 52003265), the China Postdoctoral Science Foundation (2019TQ0306) and funding from the Hefei Center for Physical Science and Technology.

Notes and references

1 K. S. Novoselov, A. K. Geim, S. V. Morozov, D. Jiang, Y. Zhang, S. V. Dubonos, I. V. Grigorieva and A. A. Firsov, *Science*, 2004, **306**, 666–669.
2 K. I. Bolotin, K. J. Sikes, Z. Jiang, M. Klima, G. Fudenberg, J. Hone, P. Kim and H. Stormer, *Solid State Commun.*, 2008, **146**, 351–355.
3 A. A. Balandin, S. Ghosh, W. Bao, I. Calizo, D. Teweldebrhan, F. Miao and C. N. Lau, *Nano Lett.*, 2008, **8**, 902–907.
4 C. Lee, X. Wei, J. W. Kysar and J. Hone, *Science*, 2008, **321**, 385–388.

5 H. Min and A. H. MacDonald, *Phys. Rev. B: Condens. Matter Mater. Phys.*, 2008, **77**, 155416.
6 E. McCann and V. I. Fal'ko, *Phys. Rev. Lett.*, 2006, **96**, 086805.
7 T. Ohta, A. Bostwick, T. Seyller, K. Horn and E. Rotenberg, *Science*, 2006, **313**, 951–954.
8 E. V. Castro, K. Novoselov, S. Morozov, N. Peres, J. L. Dos Santos, J. Nilsson, F. Guinea, A. Geim and A. C. Neto, *Phys. Rev. Lett.*, 2007, **99**, 216802.
9 Z. Li, E. Henriksen, Z. Jiang, Z. Hao, M. C. Martin, P. Kim, H. Stormer and D. N. Basov, *Phys. Rev. Lett.*, 2009, **102**, 037403.
10 C. Bao, W. Yao, E. Wang, C. Chen, J. Avila, M. C. Asensio and S. Zhou, *Nano Lett.*, 2017, **17**, 1564–1568.
11 S. Latil and L. Henrard, *Phys. Rev. Lett.*, 2006, **97**, 036803.
12 Z.-D. Chu, W.-Y. He and L. He, *Phys. Rev. B: Condens. Matter Mater. Phys.*, 2013, **87**, 155419.
13 J. L. Dos Santos, N. Peres and A. C. Neto, *Phys. Rev. B: Condens. Matter Mater. Phys.*, 2012, **86**, 155449.
14 E. J. Mele, *Phys. Rev. B: Condens. Matter Mater. Phys.*, 2010, **81**, 161405.
15 Y. Cao, V. Fatemi, S. Fang, K. Watanabe, T. Taniguchi, E. Kaxiras and P. Jarillo-Herrero, *Nature*, 2018, **556**, 43.
16 Y. Cao, V. Fatemi, A. Demir, S. Fang, S. L. Tomarken, J. Y. Luo, J. D. Sanchez-Yamagishi, K. Watanabe, T. Taniguchi and E. Kaxiras, *Nature*, 2018, **556**, 80.
17 H. Shi, Z. Zhan, Z. Qi, K. Huang, E. v. Veen, J. Á. Silva-Guillén, R. Zhang, P. Li, K. Xie, H. Ji, M. I. Katsnelson, S. Yuan, S. Qin and Z. Zhang, *Nat. Commun.*, 2020, **11**, 371.
18 X. Lu, P. Stepanov, W. Yang, M. Xie, M. A. Aamir, I. Das, C. Urgell, K. Watanabe, T. Taniguchi, G. Zhang, A. Bachtold, A. H. MacDonald and D. K. Efetov, *Nature*, 2019, **574**, 653–657.
19 Y. Jiang, X. Lai, K. Watanabe, T. Taniguchi, K. Haule, J. Mao and E. Y. Andrei, *Nature*, 2019, **573**, 91–95.
20 G. Chen, A. L. Sharpe, E. J. Fox, Y.-H. Zhang, S. Wang, L. Jiang, B. Lyu, H. Li, K. Watanabe, T. Taniguchi, Z. Shi, T. Senthil, D. Goldhaber-Gordon, Y. Zhang and F. Wang, *Nature*, 2020, **579**, 56–61.
21 D. Wong, Y. Wang, J. Jung, S. Pezzini, A. M. DaSilva, H.-Z. Tsai, H. S. Jung, R. Khajeh, Y. Kim and J. Lee, *Phys. Rev. B: Condens. Matter Mater. Phys.*, 2015, **92**, 155409.
22 A. Luican, G. Li, A. Reina, J. Kong, R. Nair, K. S. Novoselov, A. K. Geim and E. Andrei, *Phys. Rev. Lett.*, 2011, **106**, 126802.
23 G. Li, A. Luican, J. L. Dos Santos, A. C. Neto, A. Reina, J. Kong and E. Andrei, *Nat. Phys.*, 2010, **6**, 109.
24 I. Brihuega, P. Mallet, H. González-Herrero, G. T. De Laissardière, M. Ugeda, L. Magaud, J. Gómez-Rodríguez, F. Ynduráin and J.-Y. Veuillen, *Phys. Rev. Lett.*, 2012, **109**, 196802.
25 L.-J. Yin, J.-B. Qiao, W.-X. Wang, W.-J. Zuo, W. Yan, R. Xu, R.-F. Dou, J.-C. Nie and L. He, *Phys. Rev. B: Condens. Matter Mater. Phys.*, 2015, **92**, 201408.
26 G. Trambly de Laissardière, D. Mayou and L. Magaud, *Nano Lett.*, 2010, **10**, 804–808.
27 K. Kim, A. DaSilva, S. Huang, B. Fallahazad, S. Larentis, T. Taniguchi, K. Watanabe, B. J. LeRoy, A. H. MacDonald and E. Tutuc, *Proc. Natl. Acad. Sci. U. S. A.*, 2017, **114**, 3364–3369.
28 C. Pfleiderer, *Rev. Mod. Phys.*, 2009, **81**, 1551–1624.
29 H. Yoo, R. Engelke, S. Carr, S. Fang, K. Zhang, P. Cazeaux, S. H. Sung, R. Hovden, A. W. Tsen and T. Taniguchi, *Nat. Mater.*, 2019, **18**, 448.
30 Y.-H. Zhang, D. Mao, Y. Cao, P. Jarillo-Herrero and T. Senthil, *Phys. Rev. B*, 2019, **99**, 075127.
31 M. Yankowitz, S. Chen, H. Polshyn, Y. Zhang, K. Watanabe, T. Taniguchi, D. Graf, A. F. Young and C. R. Dean, *Science*, 2019, **363**, 1059–1064.
32 S. Carr, S. Fang, P. Jarillo-Herrero and E. Kaxiras, *Phys. Rev. B*, 2018, **98**, 085144.
33 B. Padhi, C. Setty and P. W. Phillips, *Nano Lett.*, 2018, **18**, 6175–6180.
34 J. Gonzalez and T. Stauber, *Phys. Rev. Lett.*, 2019, **122**, 026801.
35 A. Lopez-Bezanilla, *Phys. Rev. Mater.*, 2019, **3**, 054003.
36 F. Yndurain, *Phys. Rev. B*, 2019, **99**, 045423.
37 M. Yankowitz, J. Jung, E. Laksono, N. Leconte, B. L. Chittari, K. Watanabe, T. Taniguchi, S. Adam, D. Graf and C. R. Dean, *Nature*, 2018, **557**, 404.
38 Y. Gao, X. Lin, T. Smart, P. Ci, K. Watanabe, T. Taniguchi, R. Jeanloz, J. Ni and J. Wu, *Phys. Rev. Lett.*, 2020, **125**, 226403.
39 F. J. Culchac, R. R. Del Grande, R. B. Capaz, L. Chico and E. S. Morell, *Nanoscale*, 2020, **12**, 5014–5020.
40 G. T. De Laissardière, D. Mayou and L. Magaud, *Phys. Rev. B: Condens. Matter Mater. Phys.*, 2012, **86**, 125413.
41 E. S. Morell, J. Correa, P. Vargas, M. Pacheco and Z. Barticevic, *Phys. Rev. B: Condens. Matter Mater. Phys.*, 2010, **82**, 121407.
42 X. Fan, C. H. Chang, W. T. Zheng, J.-L. Kuo and D. J. Singh, *J. Phys. Chem. C*, 2015, **119**, 10189–10196.
43 Z. Chi, X. Chen, F. Yen, F. Peng, Y. Zhou, J. Zhu, Y. Zhang, X. Liu, C. Lin, S. Chu, Y. Li, J. Zhao, T. Kagayama, Y. Ma and Z. Yang, *Phys. Rev. Lett.*, 2018, **120**, 037002.
44 G. Kresse and J. Furthmüller, *Phys. Rev. B: Condens. Matter Mater. Phys.*, 1996, **54**, 11169.
45 J. P. Perdew, K. Burke and M. Ernzerhof, *Phys. Rev. Lett.*, 1996, **77**, 3865.
46 W. Kohn and L. J. Sham, *Phys. Rev.*, 1965, **140**, A1133.
47 G. Kresse and D. Joubert, *Phys. Rev. B: Condens. Matter Mater. Phys.*, 1999, **59**, 1758.
48 S. Grimme, *J. Comput. Chem.*, 2006, **27**, 1787–1799.
49 S. Shallcross, S. Sharma, E. Kandelaki and O. A. Pankratov, *Phys. Rev. B: Condens. Matter Mater. Phys.*, 2010, **81**, 165105.
50 C. Berger, Z. Song, X. Li, X. Wu, N. Brown, C. Naud, D. Mayou, T. Li, J. Hass and A. N. Marchenkov, *Science*, 2006, **312**, 1191–1196.
51 J. Hass, F. Varchon, J.-E. Millan-Otoya, M. Sprinkle, N. Sharma, W. A. de Heer, C. Berger, P. N. First, L. Magaud and E. H. Conrad, *Phys. Rev. Lett.*, 2008, **100**, 125504.

52 J. L. Dos Santos, N. Peres and A. C. Neto, *Phys. Rev. Lett.*, 2007, **99**, 256802.
53 Z. Feng, X. Zhang, Y. Sakurai, Z. Wang and H. Hu, *Sci. Rep.*, 2019, **9**, 17313.
54 L. Dai, *Nat. Energy*, 2016, **1**, 16041.
55 H. Graeme, P. U. Blas and J. Hannes, *J. Chem. Phys.*, 2000, **113**, 9901–9904.
56 M. Imada and M. Kohno, *Phys. Rev. Lett.*, 2000, **84**, 143–146.
57 S. Deng, A. Simon and J. Köhler, *Int. J. Mod. Phys. B*, 2005, **19**, 29–36.
58 S. Miyahara, S. Kusuta and N. Furukawa, *Phys. C*, 2007, **460**, 1145–1146.
59 Z.-X. Shen and D. S. Dessau, *Phys. Rep.*, 1995, **253**, 1–162.
60 K. Gofron, J. Campuzano, A. Abrikosov, M. Lindroos, A. Bansil, H. Ding, D. Koelling and B. Dabrowski, *Phys. Rev. Lett.*, 1994, **73**, 3302.